Int. J. Environ. Sci. Technol. (2016) 13:2805–2816
DOI 10.1007/s13762-016-1107-z

ORIGINAL PAPER

Phenol and ammonium removal by using Fe-ZSM-5 synthesized by ammonium citrate iron source

A. Aziz[1,2] · H. Park[1,2] · S. Kim[2] · K. S. Kim[1,2]

Received: 9 September 2015 / Revised: 24 June 2016 / Accepted: 6 September 2016 / Published online: 19 September 2016

Abstract Fe-ZSM-5 zeolites are important for many applications, especially for catalysis and volatile organic carbon removal. However, the inclusion of a high content of iron in the ZSM-5 structure is hindered due to the high pH required for hydrothermal synthesis. To overcome this problem, the synthesis of Fe-ZSM-5 zeolites with a novel iron chelate complex as the iron source (ammonium iron citrate) and a common iron source (iron chloride) was investigated. The synthesized materials were characterized by XRD, BET, SEM, FTIR, XPS and ICP. The total iron content was determined by ICP. Fe-ZSM-5 zeolites prepared by the ammonium iron citrate source method contain the highest iron concentration within the framework of a Mobil five structure, which has a high surface area and crystallinity. The prepared materials were used to remove phenol and ammonium. The catalytic results demonstrated that Fe-ZSM-5 prepared with ammonium iron citrate is the best catalyst.

Keywords Fe-zeolite · Chelate compound · Hydrothermal synthesis · Pollutant removal

Editorial responsibility: M. Abbaspour.

Electronic supplementary material The online version of this article (doi:10.1007/s13762-016-1107-z) contains supplementary material, which is available to authorized users.

✉ K. S. Kim
kskim@kict.re.kr

[1] University of Science and Technology Korea (UST), 217 Gajeong-ro, Yuseong-gu, Daejeon 305-350, Korea

[2] Environmental and Plant Engineering Research Institute, Korea Institute of Civil Engineering and Building Technology, 283 Goyangdae-ro, Ilsanseo-gu, Goyang-Si, Gyeonggi-do 411-712, Korea

Introduction

ZSM-5 zeolites are unique because of their high thermal stability; surface area; cation-exchange capacity; micro, meso, and macro pores; and many other qualities, and they have demonstrated usefulness as adsorbents and catalysts (Martínez and Corma 2011). During heterogeneous catalysis and adsorption, the presence of transition metals in the framework of zeolite is important because they increase its activity (Ali et al. 2013; Herman et al. 1975; Klier 1988; Smeets et al. 2010). Therefore, various researchers have investigated transition metal zeolites (George et al. 1991; Goursot et al. 2003). ZSM-5, as a type of zeolite, exhibits excellent redox and ion exchange properties; hence, it is similar to many other types of zeolites. Transition metal-ZSM-5 zeolites have also been known and studied for many years by a number of scientists (Goursot et al. 2003; Melián-Cabrera et al. 2005; van de Water et al. 2003). The transition metal-ZSM-5 has attracted attention because it has demonstrated good properties for the removal of inorganic and organic pollutants (Ali et al. 2013; Gonzalez-Olmos et al. 2012; Huang et al. 2006; Ismagilov et al. 2008; Joyner and Stockenhuber 1999; Le Van Mao et al. 1990). The incorporation of different transition metals, including Ge, Co, Cu, Zn, Ni, Fe, Mo, Ti and V, among others, into ZSM-5 has been evaluated (Ali et al. 2013; Feng and Hall 1996; Round et al. 1997; Moliner 2012; Rakshe et al. 1996; Sárkány 2002; Smeets et al. 2010). Among these transition metals, more focus was given to Fe because it has higher activity than any other metal-ZSM-5 (Long and Yang 2002), excellent thermal stability in H_2O and SO_2 media (Feng and Hall 1996), and highly selective catalytic reduction (SCR) of nitrogen oxides (NO_x) (Rutkowska et al. 2014; Shi et al. 2013) and volatile organic carbons (VOCs), as well as other favorable characteristics

(Feng and Keith Hall 1997). The insensitivity of Fe-ZSM-5 toward phosphates also separates it from all other zeolitic materials (Gonzalez-Olmos et al. 2012; Ikhlaq et al. 2012; Ismagilov et al. 2008; Kanthasamy and Larsen 2007). The reactivity and stability of the Fe-ZSM-5 adsorbent depend on the quantity of Fe ions in the ZSM-5 MFI structure. Hence, different protocols have been used to prepare Fe-ZSM-5 so that it contains the maximum possible Fe level in the crystal lattice without affecting the MFI structure (Patarin et al. 1990). Among the many procedures used for the maximum incorporation of Fe into the ZSM-5 framework, two methods are commonly used. The first method is the incorporation of iron during synthesis, and the second method employs a post-synthesis treatment (Battiston et al. 2003; Long and Yang 2001a, b). Researchers have most commonly used the post-synthesis method because of its simplicity. Post-preparation incorporation was also performed by many methods, such as ion exchange, sublimation and dry mixing with iron salts, which were followed by calcinations (Park et al. 2008; Rutkowska et al. 2014). All of these methods have a limitation for the maximum exchange of iron with aluminum. Because it is not possible to exceed the Al concentration, the maximum exchange ratio of Al/Fe that can be obtained is one. The exchange of Fe with Al in addition to its surface deposition/coating in the oxide form makes it difficult to achieve an exchange ratio of one (Kim et al. 2013; Park et al. 2008). Different researchers have used many alternatives to incorporate a high iron content into the ZSM-5 framework during synthesis, but iron was deposited on the surface or between the channels in most of these studies. Among these studies, a vast majority used iron chloride as the iron source for Fe-ZSM-5 synthesis in addition to other salts, such as iron nitrate, iron sulfate and iron acetate, among others (Nechita et al. 2005; Park et al. 2008; Rauscher et al. 1999; Rutkowska et al. 2014). These cited studies and many others also encountered the obstacle of incorporating a high content of iron into the framework because ZSM-5 crystal growth is only possible at a basic pH; however, at a high alkaline pH, iron creates precipitates, which interfere with ZSM-5 zeolite crystal growth, resulting in low crystallinity and a small quantity of iron in the MFI crystal structure (Ma et al. 2013; Szostak et al. 1987). Various scientists attempted to overcome this problem using a multistep synthesis procedure and different starting materials. However, this obstacle cannot be completely eradicated (Chen and Sachtler 1998; Feng and Keith Hall 1997; Schwidder et al. 2005). The ultimate goal of all researchers has been to support the high content of catalytic metal in its most dispersed form so that more activity for catalytic oxidation could be achieved.

The objectives of the present work were to: (1) synthesize a ZSM-5 type of porous material with a higher iron content without deforming the Mobil five (MFI) structure of ZSM-5, (2) observe the catalytic effect of the Fe-ZSM-5 prepared by ammonium iron citrate (AIC) on the catalytic removal of phenol and ammonium in water, (3) investigate the stability (reusability) of the Fe-ZSM-5 zeolite catalyst, and (4) compare Fe-ZSM-5(AIC) with Fe-ZSM-5 prepared using $FeCl_3$. To the best of our knowledge, no study has used ammonium iron citrate as an iron source to prepare a Fe-ZSM-5 zeolite catalyst.

Materials and methods

Synthesis of ZSM-5

ZSM-5 zeolite was synthesized according to the procedure described here. Silica sol (SiO_2 40 %), sodium hydroxide (NaOH), sodium aluminate ($NaAlO_2$), H_2O and tetrapropylammonium hydroxide (TPAOH) were used to synthesize ZSM-5 as reported in the literature (Narayanan et al. 1995). In the current study, ZSM-5 was prepared by dissolving 0.7481 g of $NaAlO_2$ and 1.5968 g of NaOH in 65 ml of H_2O in a plastic boat.

Silica sol (30 ml) was transferred to a beaker, and 6 ml of TPAOH was added dropwise together with the previously dissolved solution into the silica sol with continuous stirring. The molar composition of the synthesis mixture was 1 Al_2O_3:50.4 SiO_2:6.2 Na_2O:1.5 TPAOH:1248 H_2O. The gel solution was allowed to age at 50 °C and 200 rpm of stirring in an incubator for three days. The mixture was then transferred to a steel autoclave lined with Teflon for the hydrothermal reaction at 180 °C for three days under autogenous pressure. After three days, the product was collected, followed by filtration and washing until the filtrate pH reached 8.0. The solid material was oven-dried at 100 °C for 5 h. The dried material was calcined at 550 °C for 6 h and thoroughly characterized. A general schematic diagram of ZSM-5 synthesis is shown in (Aziz and Kim 2015) figure S1. The sample was coded as A.

Preparation of Fe-ZSM-5 with AIC (iron chelate complex) and $FeCl_3$ (iron salt)

Two different compounds were used to incorporate the iron contents into ZSM-5. First, iron species were incorporated prior to the hydrothermal reaction of ZSM-5 during gel formation. In a typical in situ synthesis process, all of the steps were similar to the synthesis of ZSM-5, as stated in "Synthesis of ZSM-5" section; the only the difference was that 2 g of AIC (ammonium iron citrate is a chelate compound that is soluble, even at the high pH of 8–10) and 2 g of $FeCl_3{\cdot}6H_2O$ were separately dissolved in 20 ml of H_2O; then, they were mixed with continuous stirring with silica

sol in addition to the other solutions mentioned in "Synthesis of ZSM-5" section. The samples that had similar molar ratios of the iron sources, AIC and $FeCl_3$, were named B and C, respectively.

Characterization

A Rigaku D/Max-2500 X-ray diffractometer with Cu K_α and a Ni filter was utilized to investigate the crystallinity and MFI structure of the ZSM-5 samples. The diffraction patterns were obtained between the 2θ angles over the range of 5°–50° with a scanning speed of 3°/min.

A PerkinElmer Fourier transform infrared (FTIR) spectrometer was used with KBR pellets to indicate the presence of iron in the ZSM-5 zeolites. The samples were recorded with a single-beam spectrometer with 60 added scans at a 2 cm^{-1} resolution.

A Kratos Axis Ultra XPS instrument with a monochromatic Al K_α X-ray source was used to confirm the presence of iron in the ZSM-5 samples. The analysis was performed at a low pressure of 1.33×10^{-7} Pa. First, a full energy survey scan was performed from 0 to 1250 eV. Then, scans for Si (2p), Al (2p) and Fe (2p) were performed over the energy range of the individual metal.

The ZSM-5 zeolite surface was monitored by scanning electron microscopy (SEM) (Hitachi S-4800, Japan). The dried samples were finely ground and coated with a gold–platinum alloy by ion sputtering with the help of an E-1045 Hitachi ion sputter. The images were then obtained. Energy-dispersive X-ray (EDX) mapping was also performed, and the images were recorded with a transmission electron microscope (TEM).

For the BET surface area measurement, N_2 adsorption was performed at 77 K in a Gemini series Micromeritics 2360 instrument. Samples were previously degassed at 473 K for 2 h with a Micromeritics FlowPrep 060. The BET method was used to calculate the total surface area of the prepared materials, which is used for comparison.

A PerkinElmer (Optima 7300 DV) inductively coupled plasma optical emission spectrometer (ICP-OES) was used to analyze the total content of Fe in the ZSM-5 samples. All samples were dissolved in HF and neutralized with $NaBO_3$ before analysis. One blank and four calibration standard solution samples of known Fe concentrations were prepared. The actual concentration of the Fe in the prepared ZSM-5 samples was obtained from the working calibration curve generated from the four standard solutions of Fe.

The concentrations of phenol and ammonium were measured using a UV–Vis spectrophotometer (HACH/DR4000) by measuring the absorption with Hach Program 2900 phenols and 2400 N-ammonia. The estimated detection limit for program number 2900 is 0.001 mg/L phenol, and that for 2400 is 0.017 mg/L ammonium.

Phenol and ammonium removal

The synthesized catalysts were used for the oxidation of phenol in water. This was performed in batch experiments. Phenol was purchased from Fisher Scientific in solid form and was dissolved in demineralized water to the desired concentration. Hydrogen peroxide (30 %, w/v) and all other reagents were purchased from Merck and were used as received. Experiments were performed at room temperature in a 1 L open and undivided cylindrical glass cell equipped with a pH meter and continuous stirring immersed into the solution under study. The contents were continuously stirred using a magnetic stirrer. One gram of catalyst (as a source of ferrous ion) was added after adjusting the pH to the desired value of 5, and the pH of the solution was not controlled during the reaction. Then, hydrogen peroxide, at a concentration of 300 mg/L, was added. The concentration of phenol was measured after regular intervals and a maximum of one day.

Similarly, the prepared zeolite materials were used to remove ammonium in water. The batch experiment was performed in the experimental setup discussed above. Catalyst (0.5 g) was added to the 500 mL solution containing ammonium (20 mg/L) with continuous mixing. The concentration of each stirred sample was monitored at different time intervals. The removal ($X_{\mathrm{x\ =\ phenol/ammonium}}$, %) is defined (Jiang et al. 2015) as follows:

$$X_{\mathrm{X}} = \frac{C_{\mathrm{xattimezero}t0} - C_{\mathrm{xattime}t}}{C_{\mathrm{xattimezero}t0}} \times 100\,\% \tag{1}$$

Adsorption isotherms

The isotherm data obtained for phenol and ammonium removal were analyzed using the Freundlich and Langmuir adsorption isotherm equations. The parameters for both isotherms were deduced, and the respective correlation coefficients were calculated. The linear forms of the Freundlich and Langmuir isotherms are presented below.

$$\log q_{\mathrm{e}} = \log k_{\mathrm{F}} + \frac{1}{n}\log C\mathrm{e} \tag{2}$$

$$\frac{C\mathrm{e}}{q_{\mathrm{e}}} = \frac{1}{q_{\mathrm{m}} K_{\mathrm{L}}} + \frac{C\mathrm{e}}{q_{\mathrm{m}}} \tag{3}$$

where q_{e} and $C\mathrm{e}$ are the equilibrium pollutant (phenol or ammonium) concentration on the adsorbent (mg/g) and in the solution (mg/L). k_{F} and n are the Freundlich's constant, q_{m} is the adsorption capacity (mg/g), and k_1 is the binding constant (L/mg) (Wahab et al. 2010). An adsorption isotherm study was conducted for sample B alone by stirring

0.5 g of catalyst in 500 mL solution with different initial concentrations of pollutants for 24 h.

Adsorption kinetics

To obtain the adsorption kinetic parameters, the adsorption data were analyzed using pseudo-first and pseudo-second-order kinetic models. The linear form of the Lagergren equation for pseudo-first and second-order models are given as:

$$\ln(q_e - q_t) = \ln q_e - k1t \quad (4)$$

$$\frac{t}{q_t} = \frac{1}{k2q_e^2} + \frac{t}{q_e} \quad (5)$$

where q_e (mg/g) and q_t (mg/g) are the adsorption capacity at equilibrium and time t (min), k_1 (min^{-1}) is the binding constant (J mol^{-1} K^{-1}) for the pseudo-first-order kinetic model, and k_2 (g mg^{-1} min^{-1}) is the rate constant for the pseudo-second-order kinetic model. The values of the adsorption capacity and constants (k_1 and k_2) can be calculated from the slope and intercept, respectively (Wang et al. 2011).

Results and discussion

XRD

The XRD patterns of the Fe-ZSM-5 samples together with the reference ZSM-5 are shown in Fig. 1. This figure shows that all samples (B–C) of iron-containing ZSM-5 have the typical characteristics of the MFI structure of ZSM-5 because all samples were compared with the reference XRD pattern of pure ZSM-5 (Joyner and Stockenhuber 1999; Kanthasamy and Larsen 2007). Sample A has a singlet at 2θ = 22°–24°, 30° and 45.6°, while the other samples (B and C) have doublets at the same angle of 2θ, indicating that the crystal system was changed, possibly due to the incorporation of Fe into the lattices of the zeolites. In addition, the major diffraction pattern lines of the MFI structure of ZSM-5 appeared at 2θ = 22°–25°, while the intensity of these lines increased more in sample B (Fe-ZSM-5 prepared by AIC) compared with the other samples, which possibly indicates better crystallinity. Sample C showed additional low-intensity lines at 2θ = 24.8° and 42.2°–4°, suggesting the presence of Fe_2O_3 in sample C at an extra-framework position, which could be from the agglomeration of Fe during synthesis because the $FeCl_3$·$6H_2O$ salt was used as the Fe source. No indication of an extra Fe_2O_3 framework was observed in the diffractogram of sample B.

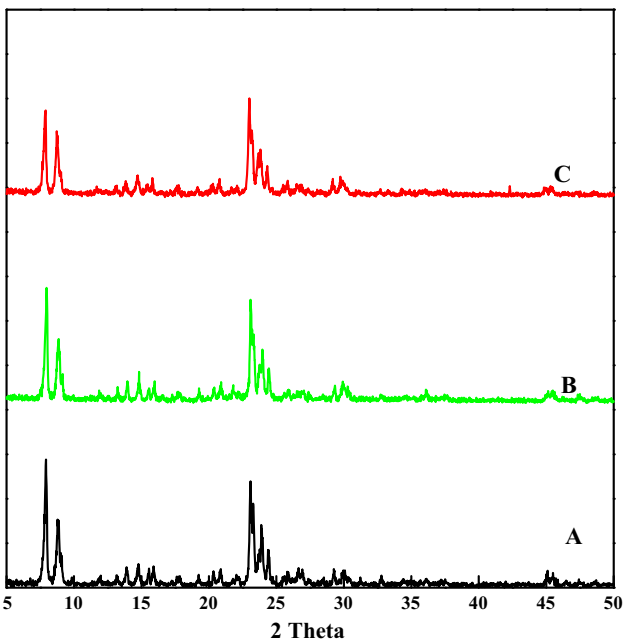

Fig. 1 XRD pattern of the synthesized samples. *a* ZSM-5, *b* Fe-ZSM-5 prepared with AIC and *c* Fe-ZSM-5 prepared with $FeCl_3$

BET

The BET surface area of the four samples was measured using N_2 adsorption isotherms at 77 K, and the results are displayed in Table 1. The pure ZSM-5 sample showed the highest BET surface area of 400 m^2/g, while the lowest BET of 186 m^2/g was found for sample C, which was synthesized with $FeCl_3$ salt. The B sample has the second highest BET surface area, indicating that the prepared material is the best of the modified samples in this study in terms of iron inclusion in the crystal system. The observed BET surface area of the zeolite materials was similar to that previously reported in the literature.

ICP

The total Fe content was measured by ICP-OES and is presented in Table 2. Table 2 shows that 1.51 % of Fe is present in sample B, which is 58 % of the added iron. Sample C contains 54 % of the added Fe. The iron on the surface or in the channels is mostly in the trivalent form

Table 1 Physicochemical properties of ZSM-5 materials

Sr #	Sample ID	BET (m^2/g)	Pore volume (cm^3/g)	Pore diameter (nm)	Fe content after phenol oxidation
1	A	400	0.1348	4.2	–
2	B	357	0.1446	2.1	>1 mg/L
3	C	186	0.9684	3.0	30 mg/L

Table 2 Results of ICP and EDX along with added metal. All numbers are given as % values

Sr #	Sample ID	Added metals						ICP (±0.05 %)					
		Si	Al	Fe	Si/Fe	Si/Al	Al/Fe	Si	Al	Fe	Si/Al	Si/Fe	Al/Fe
1	A	36.0	1.00	–	–	36.0	–	35.60	1.01	–	35.24	–	–
2	B	36.0	1.00	2.60	13.84	36.0	0.38	36.20	0.50	1.51	72.40	23.97	0.33
3	C	36.0	1.00	2.60	13.84	36.0	0.38	35.80	0.80	1.40	44.75	25.57	0.57
								EDX (±0.05 %)					
1	A	36.0	1.00	–	–	36.0	–	36.20	1.8	–	20.11	–	–
2	B	36.0	1.00	2.60	13.84	36.0	0.38	36.58	1.20	2.30	30.48	15.90	0.52
3	C	36.0	1.00	2.60	13.84	36.0	0.38	38.37	1.40	2.00	27.40	19.19	0.70
								XPS					
1	A	36.0	1.00	–	–	36.0	–	36.92	1.27	–	29.07	–	–
2	B	36.0	1.00	2.60	13.84	36.0	0.38	37.63	0.64	0.17	58.80	221.35	3.76
3	C	36.0	1.00	2.60	13.84	36.0	0.38	42.45	2.74	0.47	18.14	90.31	4.97

(Fe_2O_3) and may be less reactive toward oxidation reactions for removing organic contaminants from aerosol and wastewater streams. These ICP results are in accordance with the BET results. Sample B has the highest BET with the highest content of Fe, providing evidence that there is no structural change in ZSM-5. Sample C has the lowest BET with nearly the same Fe level as sample B as well as a low BET surface area, suggesting that more pores are blocked with iron oxide deposits. Hence, these techniques confirmed that sample B, prepared by the iron chelating complex, has a high Fe content, with the characteristic structure of ZSM-5, as well as a high surface area.

SEM

The SEM images of the prepared zeolites are shown in Fig. 2. Sharp crystals can be observed for samples A and B. Sample C had crystals of different sizes, ranging from 1 to 5 μm, with amorphous agglomerated Fe oxides. The visualized surfaces of samples A and B were cleared, indicating that no surface deposition occurred.

Elemental mapping of aluminum and iron using EDX was also applied to the ZSM-5 samples, and the results are displayed in Fig. 2. The EDX mapping images show that silicon (not shown in figure) and aluminum are properly distributed throughout the crystallized samples with a small depletion of aluminum in sample B, reflecting the possible replacement of Al with iron. Differences for the Fe distribution in two samples (B–C) were observed. For the AIC ZSM-5 sample (B), Fe appears to be uniformly distributed throughout the crystal at a low concentration. In contrast, sample C, which was prepared by $FeCl_3$, shows a much higher aggregation of Fe oxides due to agglomeration on the surface of ZSM-5. Based on these images, Fe was may be incorporated into the ZSM-5 cell through the AIC method, as it has no surface coatings. Moreover, the Si, Al, and Fe levels and their ratios in the products were determined by EDX, and the results are presented in Table 2. These concentrations and ratios did not correspond to the data of the other techniques because SEM and EDX provide information that is only based on the surface. The metal that was incorporated into the framework may be not visible on the surface, but is present; as a result, the findings are similar.

FTIR

The symmetric vibration bands of ZSM-5 and the iron-containing ZSM-5 zeolite samples are shown in the IR spectra in Fig. 3. It was previously reported (Szostak and Thomas 1986) that the IR vibration bands of the zeolite frameworks appear from 400 to 1200 cm^{-1}; furthermore, it was cited that symmetric and asymmetric vibrations occur over the range of 600–900 cm^{-1}. The hydroxyl groups attached to the ZSM-5 surface are also of utmost importance for the reactivity and chemistry of these materials; therefore, they are also identified and characterized by FTIR. The vibration bands of these surface hydroxyls usually appear between 3200 and 3800 cm^{-1}. Hence, all materials were studied over these ranges of the infrared spectrum. Figure 3 depicts the well-established ZSM-5 structural framework vibrations, lattice vibrations and hydroxyl bands.

In figure S3, the spectra of framework vibrations show double-ring vibrations at 450 cm^{-1}, a T–O bend as well as external linkage at 550 cm^{-1}, an external asymmetric

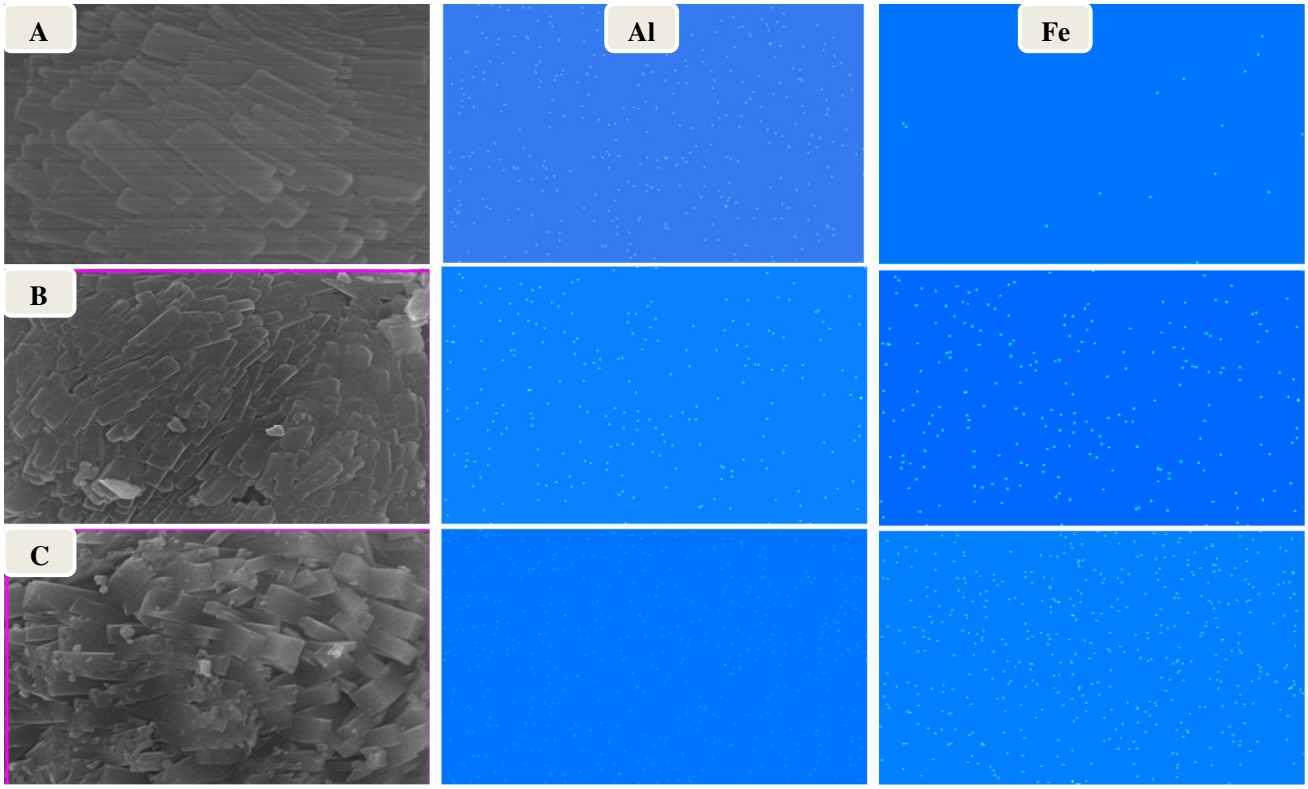

Fig. 2 SEM images (at the same size of 2 μm) and EDX mapping images. **a** ZSM-5, **b** Fe-ZSM-5 prepared with AIC and **c** Fe-ZSM-5 prepared with $FeCl_3$

stretch at 800 cm^{-1} and a very intense pore opening vibration at 1100 cm^{-1} of pure ZSM-5. Sample B has all of the other bands with little change in the position of the T–O bend as well as an external linkage from 550 to 600 cm^{-1}, suggesting the replacement of an atom with a T atom, such as Fe. The increased intensity of the external asymmetric stretch and appearance of new band at 950 cm^{-1}, which is called typical lattice vibration, indicates the substitution of Si or Al framework by another T atom, which is Fe in our case. Sample C has also a similar band at 950 cm^{-1} and less shifting of the T–O bend external linkage vibration, suggesting that some framework and T atoms are replaced with other atoms at a lower quantity.

Based on figure S4, the spectra of the OH groups indicate that two bands are assigned to the vibrations of OH groups attached to the extra-framework T atom containing species at 3680 cm^{-1} and Si–OH in defects bonded by hydrogen bonding to framework oxygen at 3500 cm^{-1} of ZSM-5 (A). The preparation of ZSM-5 with AIC and $FeCl_3$ resulted in the disappearance of the corresponding bands for the extra-framework T atom OH group and hydroxyl nests (3680 and 3500 cm^{-1}). Therefore, it may be that the Si/T atoms that are bonded via an oxygen atom to additional Si/T atoms and OH groups of hydroxyl nests are more viable for replacement with new T atoms, such as Fe. The appearance of new bands at 2880 and 2920 cm^{-1} is also observed in all samples except the pure ZSM-5 catalyst, showing that the presence of Fe(II) must not be in the framework and may be undesirable. Based on these results, there may be a certain level of Fe inclusion in the framework of the zeolite C, and with the extra-framework, there may be more surface deposition because of the precipitation of Fe at high pH during synthesis. More Fe inclusion in the lattice system of ZSM-5 zeolite was observed in catalyst B. The extra-framework inclusion of Fe is in the order AIC > $FeCl_3$ (figure S3); in the framework order according to FTIR, the order is AIC > $FeCl_3$ (figure S4). The FTIR findings corroborated the previously discussed results previously (Dey et al. 2013; Szostak et al. 1987).

XPS

The XPS results of all of the synthesized materials in the Fe (2p), Si (2p) and Al (2p) regions are presented in Fig. 4, S5 and S6, respectively. Fe gives peaks in the binding energy (BE) region of 706–711 eV (Kanthasamy and Larsen 2007) and more profoundly at 710–711 eV. A distinctive Fe (2p) peak was observed at a binding energy of 710 eV for

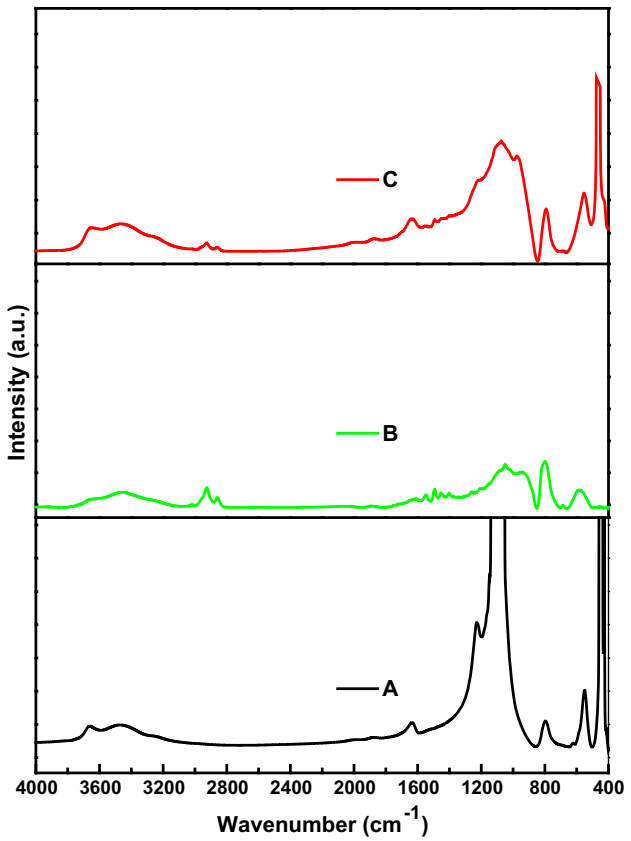

Fig. 3 FTIR spectra of *a* ZSM-5 and *b* Fe-ZSM-5 prepared with AIC and *c* Fe-ZSM-5 prepared with iron chloride

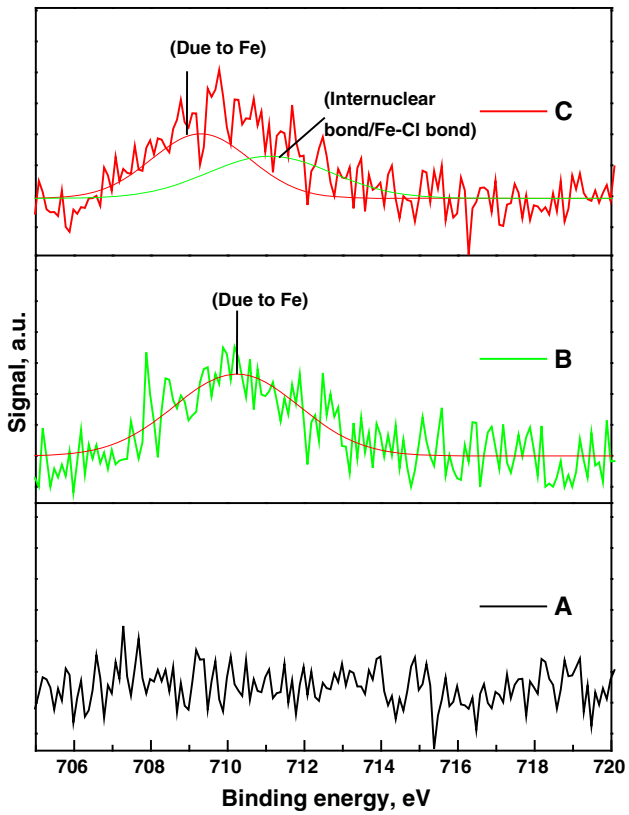

Fig. 4 XPS 2p spectra of Fe for *a* ZSM-5 and *b* Fe-ZSM-5 prepared with AIC and *c* Fe-ZSM-5 prepared with iron chloride

sample B, which is characteristic of the Fe ion, while sample C has major peaks at a binding energy of 709.5 eV, which is 0.5 eV lower than the sample B peak, as well as shoulder peaks at different binding energies, indicating that sample C contained Fe with an internuclear bonding/Fe–Cl bond. The reference ZSM-5 sample A did not have any peaks in the Fe (2p) region of the spectra.

Figure S5 shows the effect of Fe incorporation into the ZSM-5 material on the Al (2p) binding energy in the Al (2p) region of the XPS spectra. Pure ZSM-5 showed an Al (2p) peak at 74 eV with a maximum intensity, while the peak intensity of sample B was low, supporting the idea that most of the Al of ZSM-5 was replaced with Fe. Similarly, the XPS plot of sample C showed an Al (2p) peak intensity between the reference and sample B peak intensities (Jalil et al. 2005).

Figure S6 shows the Si (2p) region of the XPS spectra for all samples. In figure S6, it is clearly revealed that all samples have the typical Si (2p) peak at the binding energy region of 103 eV. However, in samples B and C, the Si (2p) peak shifted from 103 eV to 102.6 and 102.7 eV, respectively, toward a lower binding energy. This shift in the binding energy of Si (2p) provides evidence for the presence of Fe near Si. As previously discussed, Fe gives a peak at a BE of ~710 eV, which is well below the Si peak; therefore, as Fe became part of the ZSM-5 lattice, it had an effect on the Si peak, driving it toward the lower binding energy. Sample B has a high shift in the binding energy (0.4 eV), indicating that it has more iron than sample C, which reduced the BE by 0.3 eV.

The atomic ratios of iron, silicon and aluminum with respect to each other for all samples have also been obtained, as shown in Table 2. All data were computed from the spectral integral intensities of the Fe 2p, Si 2p and Al 2p lines by considering their atomic sensitivity factors. The surface atomic Si/Al and Si/Fe ratios for the B sample were much higher than in the C sample, while the Al/Fe ratio for sample B is lower than for sample C. On the other hand, nominal silicon and iron levels were initially observed at the same level. This indicates, that the AIC procedure allows for the introduction of much more iron into the framework position than for $FeCl_3$. The Al/Fe atomic ratio is 2 and 1.3 times higher for B and C, respectively, which supports the above statements. Based on these observations, the following order for the extra-framework inclusion of Fe can be suggested: C > B. By contrast, sample B has more iron in the framework than extra-framework material.

Fe-containing ZSM-5 zeolites were synthesized using three different procedures to incorporate the iron species into the framework of the ZSM-5 structure without affecting its characteristics. Extensive instrumental characterization of the prepared zeolites showed that the Fe-containing ZSM-5 zeolites that were prepared by different methods had different identities and distributions of the Fe species. The SEM–EDX mapping suggested that the iron was distributed differently in sample C, demonstrating various regions of aggregation. In contrast, the iron in the AIC ZSM-5 sample was uniformly distributed with a certain level of Al depletion, indicating the replacement of Al by Fe, as shown in Fig. 2. EDX mapping showed a small quantity of added Fe in sample B compared with the other samples because it only provides surface information. XRD, FTIR, XPS and BET revealed that the iron is incorporated into the MFI structure of ZSM-5 in the AIC ZSM-5 sample without surface deposition, while there was a surface coating/loading of iron in the form of Fe_2O_3 in sample C, which was undesired in this study. The ICP results confirmed that the iron content was 1.5 wt% for sample B. This result contradicted the EDX mapping results, but supported the XRD, FTIR and XPS findings. Researchers have reported a higher concentration of Fe in ZSM-5, but the Fe was mostly surface coated/deposited or trapped in the regular characteristic pores and channels of ZSM-5. The iron on the surface or in the channels is primarily in the mix valent form and may be less reactive in oxidation reactions for removing organic contaminants from aerosol and wastewater streams. Furthermore, the overall results of our study were based on the materials after calcinations (thermal treatment). Therefore, it is confidently demonstrated that the prepared materials were stable at a high temperature. In other studies for which there was a high content of iron incorporated into ZSM-5, the zeolite was simply loaded with iron and was used without any high-temperature thermal treatment; therefore, those materials most likely could not be regenerated.

Phenol removal

Fenton oxidation experiments were performed to enumerate the catalytic influence of different prepared ZSM-5 catalysts. The H_2O_2 concentration was kept constant at 300 mg/L, and the pH was maintained at a pre-optimized value of 5. All experiments were performed in triplicate, and the figure shows the average values.

In Fig. 5, catalyst B showed the maximum activity with a degradation efficiency of 65 % in the first 4 h and more than 80 % after 24 h. Catalyst sample C has a catalytic efficiency of 30 % for first 4 h and remained almost the same after 24 h.

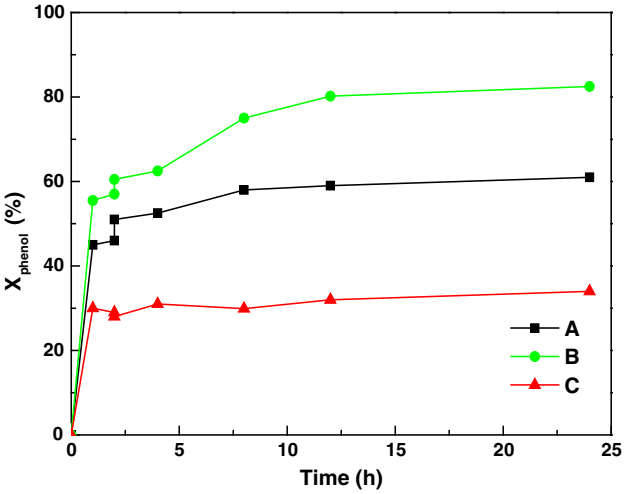

Fig. 5 Phenol removal at different time intervals using 1 g of catalyst and 300 mg/L H_2O_2 at pH 5 with continuous stirring for samples *a* ZSM-5 and *b* Fe-ZSM-5 prepared with AIC and *c* Fe-ZSM-5 prepared with iron chloride

The catalytic study indicated that the sample was prepared by a new iron source, namely AIC had the best activity with a phenol destruction efficiency of 83 %, which is very remarkable compared to all of the other prepared catalysts.

Here, the question arises as to why these types of catalysts are used in phenol degradation in addition to Fenton oxidation with the addition of iron salt. The answer is very simple and well supported by our results (Pignatello et al. 2006). By using iron salt, after Fenton oxidation, there is a sufficient quantity of iron that remained in the liquid sample, leading to sludge production, which is an additional problem that needs to be addressed. Hence, in the catalytic study, it is very important to observe the concentration of iron in the remaining liquid sample after phenol removal. Therefore, the iron content was measured after filtration, as shown in Table 1. It is already established that it is not good when the catalyst leaves behind a higher iron content due to the associated problem of sludge production (Hermosilla et al. 2009). Fortunately, our prepared catalysts have low levels of remaining iron, and catalyst sample B left the lowest possible concentration (>1 mg/L) in the liquid after Fenton oxidation compared to catalyst C, with a 30 mg/L remaining iron content. Many researchers also reported that the iron content of Fe-ZSM-5 after oxidation was similar to our result (Fajerwerg and Debellefontaine 1996). Another benefit is that it is a heterogeneous catalyst that does not require continuous feeding of peroxide, which is the case for most studied catalysts that were homogeneous. Moreover, this material released controlled iron, which was sufficient for the oxidation of phenol molecules with no excess, and the

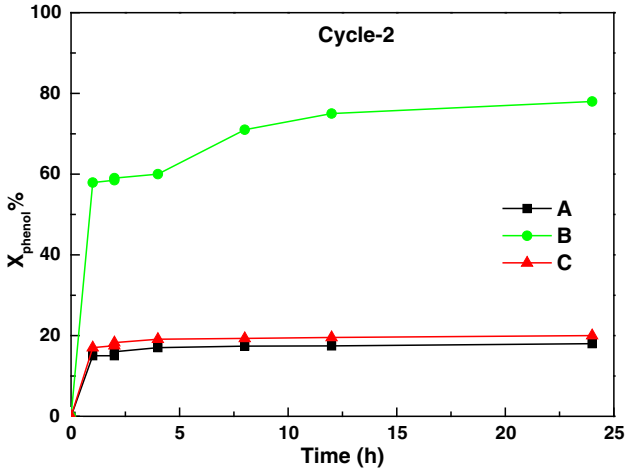

Fig. 6 Phenol removal (after regeneration at 105 °C for 3 h) at different time intervals using 1 g of catalyst and 300 mg/L H_2O_2 at pH 5 with continuous stirring for samples. *a* ZSM-5, *b* Fe-ZSM-5 prepared with AIC and *c* Fe-ZSM-5 prepared with iron chloride

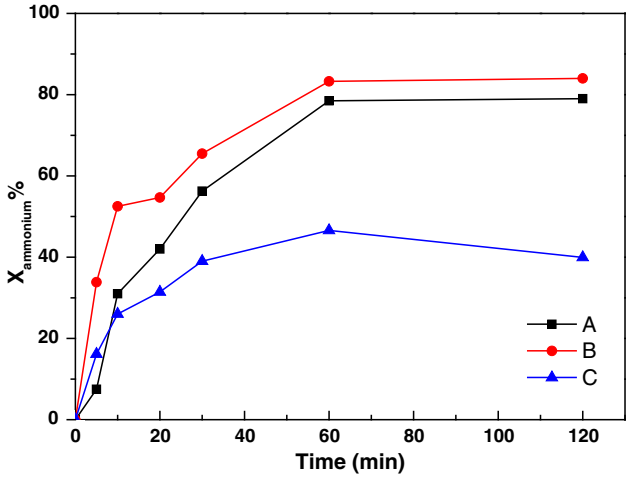

Fig. 7 Ammonia removal at different time intervals using 0.5 g of catalyst at pH 7 with continuous stirring for samples *a* ZSM-5 and *b* Fe-ZSM-5 prepared with AIC and *c* Fe-ZSM-5 prepared with iron chloride

remaining iron stayed within the catalyst structure and was possibly consumed in the next cycle by simply drying the catalyst at 105 °C for 3 h. This heating approach to dry the catalyst worked to regenerate the catalyst. The results of phenol oxidation for the next cycle after regeneration are shown in Fig. 6.

Sample B has a catalytic activity of 78 % phenol degradation, while samples A and C have activities of 18 and 20 %, respectively, which are better than previously reported, as mentioned in Table 3. The observation that sample A removes a small amount of phenol may be from adsorption on the pores and channels, as it has no iron content for Fenton oxidation; therefore, the only possibility is adsorption.

Ammonia removal

The removal of ammonia was also studied with all of the prepared materials, and its effectiveness is shown in Fig. 7. In this figure, it is evident that the sample prepared with AIC has a better removal efficiency than the sample prepared with iron chloride. Meanwhile, it is comparable to ZSM-5 with no iron, which may be because ZSM-5 has a higher BET surface area than any sample and therefore removed ammonium at a level that was almost similar to Fe-ZSM-5 prepared by AIC, but this would probably not be achievable if it is used for a 2nd cycle, which is in contrast with Fe-ZSM-5 prepared by the AIC sample. The removal capacity is higher than that reported for Fe-zeolites (Kim

Table 3 Comparison of the pollutant removal capacities of different materials

Material	Pollutant	Capacity (mg/g)	Temperature (°C)	References
Natural zeolite	Phenol	4.95	25	(Yousef et al. 2011)
Zeolite	Phenol	0.35	25	(Bizerea Spiridon et al. 2013)
Eggshell	Phenol	0.58	25	(Daraei et al. 2013)
Y-SMZ	Phenol	3.58	25	(Kamble et al. 2008)
Na-X	Phenol	100	45	(Irani et al. 2015)
ZSM-5	Phenol	2.9	25	(Aziz and Kim 2015)
Sample A	Phenol	6.90	25	Current study
Sample B	Phenol	8.45	25	Current study
Sample C	Phenol	3.40	25	Current study
Sawdust	Ammonium	1.26	25	(Wahab et al. 2010)
Zeolite	Ammonium	8.4	–	(Bolan et al. 2003)
Sample A	Ammonium	15.72	25	Current study
Sample B	Ammonium	21.12	25	Current study
Sample C	Ammonium	13.1	25	Current study

Table 4 Langmuir and Freundlich adsorption constants for phenol and ammonium by Fe-ZSM-5 prepared with AIC

Pollutants	Langmuir		Freundlich		
	R^2	K_L (L/mg)	R^2	n	k_F (mg/g)/(mg/L)$^{1/2}$
Phenol	0.9951	2.43	0.7337	3.85	5.37
Ammonium	0.9902	2.24	0.9933	6.08	14.34

Table 5 Pseudo-first- and second-order kinetic parameter constants for phenol and ammonium by Fe-ZSM-5 prepared with AIC

Pollutants	Initial conc. (mg/L)	Pseudo-first-order			Pseudo-second-order		
		R^2	q_e (mg/g)	k_1 (min^{-1})	R^2	q_e (mg/g)	k_2 g/(mg min)
Phenol	10	0.9000	6.42	0.0989	0.9917	8.58	0.079
Phenol	15	0.9025	2.65	0.0405	0.9955	7.96	0.170
Ammonium	10	0.8661	5.90	0.0248	0.9976	10.11	0.027
Ammonium	20	0.9255	18.38	0.0332	0.9942	18.89	0.004

et al. 2013; Marañón et al. 2006), as depicted in Table 3. In Figs. 6 and 7, sample B (Fe-ZSM-5, prepared by novel iron source AIC) was the best catalyst for future use in any field of catalysis.

Adsorption and kinetic studies

The experimental data for phenol and ammonium adsorption on Fe-ZSM-5 prepared with AIC were utilized to plot the linear form of the Langmuir and Freundlich models. The isotherm constants and coefficients of correlation for each adsorption model are shown in Table 4. In Table 4, the equilibrium data fit well to all of the adsorption isotherm models, except for the Freundlich model for phenol.

The k_F constant for ammonium was higher than that of phenol, as k_F, in the results showed the extent of pollutant removal; however, K_L and the correlation coefficient, R^2, were higher for phenol than ammonium, although both were greater than 0.99. This revealed that the phenol is more favorable for monolayer adsorption, while ammonium is heterogeneous (multilayer adsorption).

In Table 5, the parameters of kinetic models for phenol and ammonium adsorption onto Fe-ZSM-5 (B) are displayed. The pseudo-first and pseudo-second-order kinetic models show a linear relationship, with R^2 values ranging from 0.8661 to >0.99, respectively.

The pseudo-second-order kinetic model more accurately corresponds to the experimental data of phenol and ammonium adsorption onto Fe-ZSM-5. The correlation coefficient R^2 values are between 0.9917 and 0.9976 based on the initial concentrations of the pollutants. Moreover, it can also be noted that the values of adsorption capacities (qe (mg/g) at equilibrium are near those calculated through experimental results. Previously published studies have also presented that the pseudo-second-order kinetic model fits well for the adsorption data of pollutants, such as phenol (Bizerea Spiridon et al. 2013).

Conclusion

The conclusions of this study are as follows.

The incorporation of Fe in the framework of ZSM-5 occurs to a certain extent in all three samples prepared by different methods and ion exchange. The iron in the $FeCl_3$ method for the ZSM-5 materials (C) appeared to agglomerate compared with the iron in the AIC ZSM-5 (B) zeolites. Although ICP depicts only a slight difference in the quantity of Fe in both samples (B and C), sample C was shown to be an inferior material during characterization, as it showed substantial aggregation and more extra-framework iron as well as a low BET compared to sample B. Therefore, it is clear that the Fe-ZSM-5 prepared by the novel iron source AIC has the best characteristics with the highest Fe content (60 % of added) reported to date without any change in the properties of ZSM-5. The results of phenol and ammonium removal also supported our theory regarding the excellent catalytic ability of Fe-ZSM-5 prepared by an AIC catalyst. Therefore, it is understandable that Fe-ZSM-5 (B) material has potential regenerative applications in the fields of catalysis, volatile organic removal and wastewater treatment, among others.

Acknowledgments The authors thank the Korea Institute of Civil Engineering and Building Technology (KICT), Korea University of Science and Technology (UST), Korea (Research No 2016-0158), for help performing the research work submitted in this article.

References

Ali I, Hassan A, Shabaan S, El-Nasser K (2013) Synthesis and characterization of composite catalysts Cr/ZSM-5 and their effects toward photocatalytic degradation of p-nitrophenol. Arab J Chem 22:1401–1406. doi:10.1016/j.arabjc.2013.07.042

Aziz A, Kim K (2015) Investigation of tertiary butyl alcohol as template for the synthesis of ZSM-5 zeolite. J Porous Mater 22:1401–1406. doi:10.1007/s10934-015-0019-5

Battiston AA et al (2003) Evolution of Fe species during the synthesis of over-exchanged Fe/ZSM-5 obtained by chemical vapor deposition of $FeCl_3$. J Catal 213:251–271. doi:10.1016/S0021-9517(02)00051-9

Bizerea Spiridon O, Preda E, Botez A, Pitulice L (2013) Phenol removal from wastewater by adsorption on zeolitic composite. Environ Sci Pollut Res 20:6367–6381. doi:10.1007/s11356-013-1625-x

Bolan NS, Mowatt C, Adriano DC, Blennerhassett JD (2003) Removal of ammonium ions from fellmongery effluent by zeolite. Commun Soil Sci Plant Anal 34:1861–1872. doi:10.1081/CSS-120023222

Chen H-Y, Sachtler WMH (1998) Activity and durability of Fe/ZSM-5 catalysts for lean burn NO_x reduction in the presence of water vapor. Catal Today 42:73–83. doi:10.1016/S0920-5861(98)00078-9

Daraei H, Mittal A, Noorisepehr M, Daraei F (2013) Kinetic and equilibrium studies of adsorptive removal of phenol onto eggshell waste. Environ Sci Pollut Res 20:4603–4611. doi:10.1007/s11356-012-1409-8

Dey KP, Ghosh S, Naskar MK (2013) Organic template-free synthesis of ZSM-5 zeolite particles using rice husk ash as silica source. Ceram Int 39:2153–2157. doi:10.1016/j.ceramint.2012.07.083

Fajerwerg K, Debellefontaine H (1996) Wet oxidation of phenol by hydrogen peroxide using heterogeneous catalysis Fe-ZSM-5: a promising catalyst. Appl Catal B 10:L229–L235. doi:10.1016/S0926-3373(96)00041-0

Feng X, Hall WK (1996) On the unusual stability of overexchanged FeZSM-5. Catal Lett 41:45–46. doi:10.1007/BF00811711

Feng X, Keith Hall W (1997) FeZSM-5: a durable SCR catalyst for NO_x removal from combustion streams. J Catal 166:368–376. doi:10.1006/jcat.1997.1530

George AR, Catlow CRA, Thomas JM (1991) Determining the environment of transition metal ions in zeolitic catalysts: a combined computational and synchrotron-based study of nickel ions in zeolite-Y. Catal Lett 8:193–200. doi:10.1007/BF00764116

Gonzalez-Olmos R, Martin MJ, Georgi A, Kopinke F-D, Oller I, Malato S (2012) Fe-zeolites as heterogeneous catalysts in solar Fenton-like reactions at neutral pH. Appl Catal B 125:51–58. doi:10.1016/j.apcatb.2012.05.022

Goursot A, Coq B, Fajula F (2003) Toward a molecular description of heterogeneous catalysis: transition metal ions in zeolites. J Catal 216:324–332. doi:10.1016/S0021-9517(02)00110-0

Herman RG, Lunsford JH, Beyer H, Jacobs PA, Uytterhoeven JB (1975) Redox behavior of transition metal ions in zeolites. I. Reversibility of the hydrogen reduction of copper Y zeolites. J Phys Chem 79:2388–2394. doi:10.1021/j100589a009

Hermosilla D, Cortijo M, Huang CP (2009) Optimizing the treatment of landfill leachate by conventional Fenton and photo-Fenton processes. Sci Total Environ 407:3473–3481. doi:10.1016/j.scitotenv.2009.02.009

Huang Q, Vinh-Thang H, Malekian A, Eić M, Trong-On D, Kaliaguine S (2006) Adsorption of n-heptane, toluene and o-xylene on mesoporous UL-ZSM-5 materials. Microporous Mesoporous Mater 87:224–234. doi:10.1016/j.micromeso.2005.08.011

Ikhlaq A, Brown DR, Kasprzyk-Hordern B (2012) Mechanisms of catalytic ozonation on alumina and zeolites in water: formation of hydroxyl radicals. Appl Catal B 123–124:94–106. doi:10.1016/j.apcatb.2012.04.015

Irani M, Rad LR, Pourahmad H, Haririan I (2015) Optimization of the combined adsorption/photo-Fenton method for the simultaneous removal of phenol and paracetamol in a binary system. Microporous Mesoporous Mater 206:1–7. doi:10.1016/j.micromeso.2014.12.009

Ismagilov ZR, Matus EV, Tsikoza LT (2008) Direct conversion of methane on Mo/ZSM-5 catalysts to produce benzene and hydrogen: achievements and perspectives. Energy Environ Sci 1:526–541. doi:10.1039/B810981H

Jalil PA, Kariapper MS, Faiz M, Tabet N, Hamdan NM, Diaz J, Hussain Z (2005) Surface and bulk investigation of ZSM-5 and Al-MCM-41 using synchrotron XPS, XANES, and hexane cracking. Appl Catal A: General 290:159–165. doi:10.1016/j.apcata.2005.05.025

Jiang S, Zhang H, Yan Y, Zhang X (2015) Stability and deactivation of Fe-ZSM-5 zeolite catalyst for catalytic wet peroxide oxidation of phenol in a membrane reactor. RSC Adv 5:41269–41277. doi:10.1039/C5RA05039A

Joyner R, Stockenhuber M (1999) Preparation, characterization, and performance of Fe-ZSM-5 catalysts. J Phys Chem B 103:5963–5976. doi:10.1021/jp990978m

Kamble SP, Mangrulkar PA, Bansiwal AK, Rayalu SS (2008) Adsorption of phenol and o-chlorophenol on surface altered fly ash based molecular sieves. Chem Eng J 138:73–83. doi:10.1016/j.cej.2007.05.030

Kanthasamy R, Larsen SC (2007) Visible light photoreduction of Cr(VI) in aqueous solution using iron-containing zeolite tubes. Microporous Mesoporous Mater 100:340–349. doi:10.1016/j.micromeso.2006.11.021

Kim KS, Park JO, Nam SC (2013) Synthesis of iron-loaded zeolites for removal of ammonium and phosphate from aqueous solutions. Environ Eng Res 18:267–276. doi:10.4491/eer.2013.18.4.267

Klier K (1988) Transition-metal ions in zeolites: the perfect surface sites. Langmuir 4:13–25. doi:10.1021/la00079a003

Le Van MR, Nguyen TM, Yao J (1990) Conversion of ethanol in aqueous solution over ZSM-5 zeolites: influence of reaction parameters and catalyst acidic properties as studied by ammonia TPD technique. Appl Catal 61:161–173. doi:10.1016/S0166-9834(00)82141-7

Long RQ, Yang RT (2001a) Fe-ZSM-5 for selective catalytic reduction of NO with NH3: a comparative study of different preparation techniques. Catal Lett 74:201–205. doi:10.1023/A:1016670217673

Long RQ, Yang RT (2001b) Temperature-programmed desorption/surface reaction (TPD/TPSR) study of Fe-exchanged ZSM-5 for selective catalytic reduction of nitric oxide by ammonia. J Catal 198:20–28. doi:10.1006/jcat.2000.3118

Long RQ, Yang RT (2002) Reaction mechanism of selective catalytic reduction of NO with NH3 over Fe-ZSM-5 catalyst. J Catal 207:224–231. doi:10.1006/jcat.2002.3528

Ma L, Qu H, Zhang J, Tang Q, Zhang S, Zhong Q (2013) Preparation of nanosheet Fe-ZSM-5 catalysts, and effect of Fe content on acidity, water, and sulfur resistance in the selective catalytic reduction of NO x by ammonia. Res Chem Intermed 39:4109–4120. doi:10.1007/s11164-012-0927-9

Marañón E, Ulmanu M, Fernández Y, Anger I, Castrillón L (2006) Removal of ammonium from aqueous solutions with volcanic tuff. J Hazard Mater 137:1402–1409. doi:10.1016/j.jhazmat.2006.03.069

Martínez C, Corma A (2011) Inorganic molecular sieves: preparation, modification and industrial application in catalytic processes. Coord Chem Rev 255:1558–1580. doi:10.1016/j.ccr.2011.03.014

Melián-Cabrera I, Kapteijn F, Moulijn JA (2005) Innovations in the synthesis of Fe-(exchanged)-zeolites. Catal Today 110:255–263. doi:10.1016/j.cattod.2005.09.040

Moliner M (2012) Direct synthesis of functional zeolitic materials ISRN. Mater Sci 2012:1–24. doi:10.5402/2012/789525

Narayanan S, Sultana A, Krishna K, Mériaudeau P, Naccache C (1995) Synthesis of ZSM-5 type zeolites with and without template and evaluation of physicochemical properties and aniline alkylation activity. Catal Lett 34:129–138. doi:10.1007/BF00808329

Nechita M-T, Berlier G, Ricchiardi G, Bordiga S, Zecchina A (2005) New precursor for the post-synthesis preparation of Fe-ZSM-5 zeolites with low iron content. Catal Lett 103:33–41. doi:10.1007/s10562-005-6500-z

Park J-H, Choung J-H, Nam I-S, Ham S-W (2008) N_2O decomposition over wet- and solid-exchanged Fe-ZSM-5 catalysts. Appl Catal B 78:342–354. doi:10.1016/j.apcatb.2007.09.020

Patarin J, Kessler H, Guth JL (1990) Iron distribution in iron MFI-type zeolite samples synthesized in fluoride medium: influence of the synthesis procedure. Zeolites 10:674–679. doi:10.1016/0144-2449(90)90078-6

Pignatello JJ, Oliveros E, MacKay A (2006) Advanced oxidation processes for organic contaminant destruction based on the fenton reaction and related chemistry. Crit Rev Environ Sci Technol 36:1–84. doi:10.1080/10643380500326564

Rakshe B, Ramaswamy V, Ramaswamy AV (1996) Crystalline, Microporous Zirconium Silicates with MEL Structure. J Catal 163:501–505. doi:10.1006/jcat.1996.0353

Rauscher M, Kesore K, Mönnig R, Schwieger W, Tißler A, Turek T (1999) Preparation of a highly active Fe-ZSM-5 catalyst through solid-state ion exchange for the catalytic decomposition of N_2O. Appl Catal A 184:249–256. doi:10.1016/S0926-860X(99)00088-5

Round CI, Williams CD, Duke CVA (1997) Co-ZSM-5 and Mn-ZSM-5 synthesised directly from aqueous fluoride gels. Chem Commun 19:1849–1850. doi:10.1039/A704148I

Rutkowska M, Chmielarz L, Jabłońska M, Van Oers CJ, Cool P (2014) Iron exchanged ZSM-5 and Y zeolites calcined at different temperatures: activity in N_2O decomposition. J Porous Mater 21:91–98. doi:10.1007/s10934-013-9751-x

Sárkány J (2002) Effects of water and ion-exchanged counterion on the FTIR spectra of ZSM-5. II. (Cu + –CO)-ZSM-5: coordination of Cu + –CO complex by H_2O and changes in skeletal T–O–T vibrations. Top Catal 18:271–277. doi:10.1023/A:1013850924694

Schwidder M, Santhosh Kumar M, Bruckner A, Grunert W (2005) Active sites for NO reduction over Fe-ZSM-5 catalysts. Chem Commun 6:805–807. doi:10.1039/b414179b

Shi X, Liu F, Xie L, Shan W, He H (2013) NH_3-SCR performance of fresh and hydrothermally aged Fe-ZSM-5 in standard and fast selective catalytic reduction reactions. Environ Sci Technol 47:3293–3298. doi:10.1021/es304421v

Smeets PJ, Woertink JS, Sels BF, Solomon EI, Schoonheydt RA (2010) Transition-metal ions in zeolites: coordination and activation of oxygen. Inorg Chem 49:3573–3583. doi:10.1021/ic901814f

Szostak R, Thomas TL (1986) Reassessment of zeolite and molecular sieve framework infrared vibrations. J Catal 101:549–552. doi:10.1016/0021-9517(86)90286-1

Szostak R, Nair V, Thomas TL (1987) Incorporation and stability of iron in molecular-sieve structures. Ferrisilicate analogues of zeolite ZSM-5. J Chem Soc, Faraday Trans 1: Phys Chem Condens Ph 83:487–494. doi:10.1039/F19878300487

van de Water LGA, van der Waal JC, Jansen JC, Cadoni M, Marchese L, Maschmeyer T (2003) Ge-ZSM-5: the simultaneous incorporation of Ge and Al into ZSM-5 using a parallel synthesis approach. J Phys Chem B 107:10423–10430. doi:10.1021/jp0304531

Wahab MA, Jellali S, Jedidi N (2010) Ammonium biosorption onto sawdust: FTIR analysis, kinetics and adsorption isotherms modeling. Bioresour Technol 101:5070–5075. doi:10.1016/j.biortech.2010.01.121

Wang J, Zheng C, Ding S, Ma H, Ji Y (2011) Behaviors and mechanisms of tannic acid adsorption on an amino-functionalized magnetic nanoadsorbent. Desalination 273:285–291. doi:10.1016/j.desal.2011.01.042

Yousef RI, El-Eswed B, AaH A-M (2011) Adsorption characteristics of natural zeolites as solid adsorbents for phenol removal from aqueous solutions: kinetics, mechanism, and thermodynamics studies. Chem Eng J 171:1143–1149. doi:10.1016/j.cej.2011.05.012